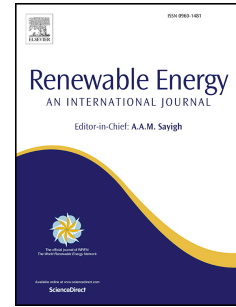


Journal Pre-proof

An experimental study of the thrust and power produced by a 1/20th scale tidal turbine utilising blade winglets

Rodolfo Olvera-Trejo, Luke E. Myers, Luke Blunden, AbuBakr S. Bahaj



PII: S0960-1481(24)00478-6

DOI: <https://doi.org/10.1016/j.renene.2024.120413>

Reference: RENE 120413

To appear in: *Renewable Energy*

Received Date: 7 February 2023

Revised Date: 1 March 2024

Accepted Date: 28 March 2024

Please cite this article as: Olvera-Trejo R, Myers LE, Blunden L, Bahaj AS, An experimental study of the thrust and power produced by a 1/20th scale tidal turbine utilising blade winglets, *Renewable Energy* (2024), doi: <https://doi.org/10.1016/j.renene.2024.120413>.

This is a PDF file of an article that has undergone enhancements after acceptance, such as the addition of a cover page and metadata, and formatting for readability, but it is not yet the definitive version of record. This version will undergo additional copyediting, typesetting and review before it is published in its final form, but we are providing this version to give early visibility of the article. Please note that, during the production process, errors may be discovered which could affect the content, and all legal disclaimers that apply to the journal pertain.

© 2024 Published by Elsevier Ltd.

1 An Experimental Study of the Thrust and Power Produced by a 1/20th Scale Tidal Turbine Utilising
2 Blade Winglets

3 Rodolfo Olvera-Trejo ^{a*}, Luke E. Myers ^a, Luke Blunden ^a, AbuBakr S. Bahaj ^a

4
5 ^a Faculty of Engineering and Physical Sciences. University of Southampton
6 University Road, Southampton, SO17 1BJ, United Kingdom
7

8 Abstract
9

10 Winglets have been employed in the aviation industry to reduce vortices generated at aircraft wings,
11 decreasing drag, and hence increasing fuel economy. For rotating applications previous experimental
12 and numerical studies addressed the application for wind turbines and suggested winglets facing
13 backwards on the suction side of a blade could increase the power capture. This paper presents
14 experimental work using a scale 3-bladed horizontal axis tidal turbine. An oil-based paint flow
15 visualisation coupled to blade thrust and torque measurements helped to identify the mechanism
16 behind the phenomenon affecting the performance of winglets facing the suction side of a turbine
17 blade. The results show that on average a winglet facing downstream decreases the power
18 coefficient 1-2% and increases the thrust coefficient up to 6% for tip speed ratios 5.0-7.0. On the
19 other hand, a symmetrically mirrored winglet facing upstream increased the power coefficient by 1-
20 2%, and the thrust coefficient by 3-4%. Further, increased bending moments at the root of the blade
21 were estimated to be in the range 4.5-6.0%. Winglets have the potential to provide a meaningful
22 increase to power capture at minimal additional capital cost without increasing rotor diameters.
23 Further work to optimise pressure-side winglets should be conducted.

24
25 Keywords: Experimental, flow visualization, marine energy, tidal turbine, winglets.
26

27 **1. Introduction**

28 Globally there are ongoing activities with targets geared to decarbonise our electricity generation.
29 Many countries have set targets to achieve an ever-increasing share of electricity production from
30 renewable energy sources to alleviate the emissions emanating from fossil fuel use. More recently
31 an additional- urgency to move to low -carbon sources was brought into sharper focus by global
32 geopolitical events – such as the war in Ukraine and its effect on gas supplies. Wholesale prices for
33 gas and electricity have increased sharply from relatively stable levels and national governments are
34 now taking security of supply much more seriously and as a driver to develop indigenous sources of
35 renewable energy electrical power generation. Previously, the EU Renewable Energy Directive [1]
36 set a target of 20% renewables by 2020 on average between member states which was recently
37 revised upwards to 45% by 2030 [2]. Similarly, the UK had a target of 30% of its electricity to be
38 produced from renewables by 2020 [1], which was achieved and exceeded in 2019, where 35% of
39 total electricity generation came from renewables. More recently, the UK announced an intention
40 of achieving 95% of its electricity from low-carbon sources by 2030, with high dependence on
41 offshore wind, solar energy, and nuclear power to support electricity supply independence and
42 security [3].
43

44 Marine energy, specifically that which arises from the kinetic energy of the flow in the oceans (tidal
45 stream and ocean currents), can contribute to renewable energy capacity, and increase diversity of
46 generation [4]. Tidal stream is also highly predictable so that power generation can be smoothly
47 integrated in power grids delivery at scale. However, as this is an emerging technology, it will need

* Corresponding author. R.Olvera@soton.ac.uk Energy and Climate Change Division, Faculty of Engineering and Physical Sciences, University of Southampton, SO16 7QF, Southampton, United Kingdom.

48 clear support mechanisms to achieve a reduction in the presently high Levelised Cost of Energy
49 (LCOE) so that it can compete with other renewables [5].

50

51 At the time of writing and in many countries, the support for marine energy technologies is
52 somewhat uncertain. However, recently the UK Government has provided a ring-fenced funding
53 support mechanism for marine energy in its fourth round of the Contracts for Difference (CfD). The
54 CfD funding guarantees a fixed price for electricity from renewables supplied to the national grid. In
55 July 2022 under the UK CfD scheme, it was announced that four free stream tidal energy projects
56 with a total installed capacity of 40.82 MW, at CfD price of £178.54/MWh will be supported [6]. This
57 must be seen in the context of a historical market price of approximately £50/MWh since 2010 as
58 compared to 2022 where the level is currently in the range £150 to £250 /MWh as a result of market
59 price volatility.

60

61 There have been several deployments of sizeable tidal turbines to date with a latter move to small
62 grid-connected farms or arrays of multiple devices. The European Marine Energy Centre (EMEC) in
63 Orkney, UK, maintains grid-connected testing berths currently serving large-scale prototype devices.
64 The most advanced projects at the time of writing are the Shetland tidal array located in Bluemell
65 sound consisting of four 100kW devices and the Meygen project located in the Inner Sound of the
66 Pentland Firth presently consisting of four devices with total rated power of 6MW. There are
67 numerous areas in waters around the British Isles and indeed worldwide with consents and
68 permissions granted for freestream tidal energy projects. The €46.8m TIGER project funded by the
69 European Interreg programme has a stated aim to support the tidal industry to reduce costs from an
70 estimated €300MW/h to €150MW/h by 2025 [7] as well as provide support for up to 8MW of
71 installed capacity at sites around the Channel region between the UK and France.

72

73 Reducing the LCOE can be achieved by reducing the capital cost of the turbines in combination with
74 maximising power generation through increased efficiency of energy conversion that can arise from
75 optimising the power capture, power-take-off and electrical subsystems. One significant gain can be
76 made from the primary power-capture subsystem which in most cases for a tidal turbine is a lift
77 force-based rotor. Common routes such as increasing rotor diameter or constructing thinner more
78 slender blades are naturally limited due to the high thrust forces per unit area and the constrained
79 depth of tidal sites.

80

81 Winglets of different designs have been employed extensively in the aviation sector and now most
82 new modern commercial aircraft have winglets present at the wing tips. Enercon, to the best of the
83 authors' knowledge, is the only wind turbine manufacturer that has invested in research that has led
84 to winglets being used on its most recent designs [8]. However, to our knowledge there is no
85 available performance data is made available in the public domain. In implementing winglets to a
86 turbine blade, blade root and tip losses are two areas that will require attention with regard to
87 increasing power capture. Further, Enercon has recently deployed blades that extend onto the hub
88 nose cone (with flow-directing surfaces on the nose cone itself) to minimise hub losses and winglets
89 at the blade tips to minimise or even negate aerodynamic tip losses.

90

91 This work focuses on the design and quantification of performance of winglets installed on a 1-metre
92 diameter model tidal turbine. The work investigates the advantages of winglets for a tidal turbine to
93 increase power capture for the same rotor diameter through a blade modification that has a
94 relatively modest cost, thus reducing the LCOE with minimal change to the overall device design.

95

96

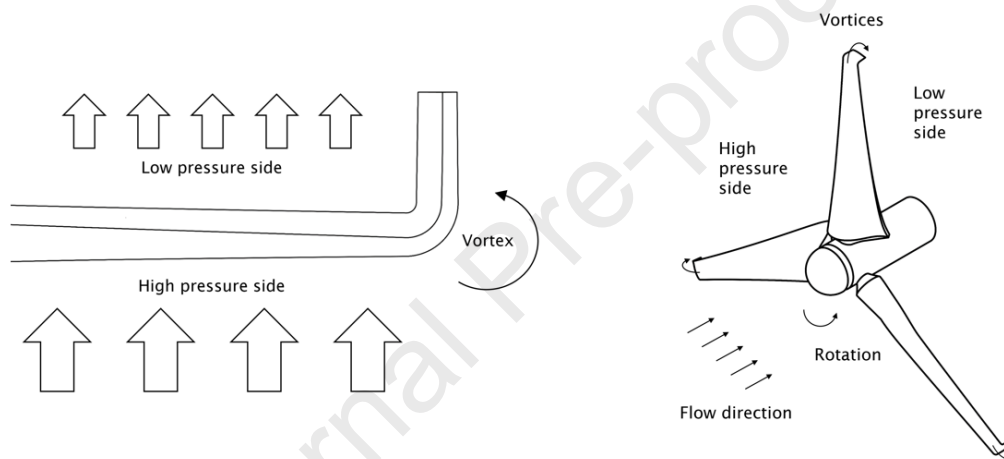
97

98

2. Review of winglet design, application and research

99
100

101 Throughout the years, different methods have been proposed to increase energy extraction from
102 turbine blades using techniques such as: micro-tabs, non-straight blades, winglets, passively
103 adaptive blades, slots, and tubercles. The most widely studied type, and probably the ones that have
104 shown better results on aeroplane wings, are winglets. In 1897, the English engineer Frederick W.
105 Lanchester obtained a patent for vertical surfaces at the wing tips. In 1976 an aeronautical engineer,
106 Richard Whitcomb, conducted research at NASA using the term winglet to refer to a nearly vertical
107 wing extension in order to reduce the induced drag on wings [9]. In principle, the winglets' main
108 function is to prevent the interaction from the high to the low-pressure sides of the wing, reducing
109 the tip vortex, whilst decreasing the spanwise flow, resulting in reducing the induced drag [10].
110 Figure 1 (Left) shows the vortex formed at the edge of a wing where the flow from the high-pressure
111 side travels towards the low-pressure side, as a result of the pressure difference. Figure 1 (Right)
112 illustrates the same vortices occurring at the turbine blade tips. In contrast to an aeroplane wing,
113 where vortices are perpendicular to the stream flow, for rotating turbines (wind or tidal), the
114 vortices travel in the same direction as the fluid.



115
116

Figure 1. Left: Vortex direction on an airplane wing. Right: Tip vortices on a tidal turbine.

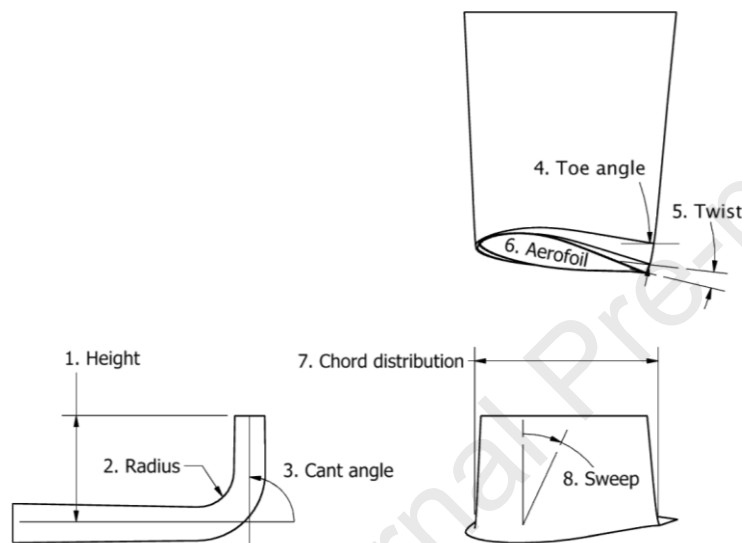
117 Early work, in 1985 [11], which tested tip devices on a horizontal axis wind turbine found no
118 apparent improvement over the regular wing performance. The work emphasized that *'The*
119 *promising results obtained on nonrotating wings make it difficult to accept that tip devices could not*
120 *improve wind turbine performance'*. Mie University, in collaboration with Delft University of
121 Technology (DUT), carried out a series of experiments on "Mie-type" winglets [12]. The "Mie-type"
122 vanes of approximately 20% of the height of the blade were tested and an increase in the power
123 coefficient (C_p) of around 27% for a blade Tip Speed Ratio (TSR) of 4 was reported. After that, Van
124 Bussel [13] developed a momentum theory for a blade-winglet configuration. The main assumption
125 was that the increase in power was due to the shift in the vorticity of the wake downstream. Further
126 experiments and an adjusted theoretical model were then reported showing a 17% increase in
127 power coefficient for a tip speed ratio of 5. Other studies in 2003 were conducted and a power
128 augmentation of 8.75% was reported [14].

129

130 Later in 2006/07 Johansen, Sørensen and Gaunna [15] used Computational Fluid Dynamics (CFD) to
131 investigate the possible increase in C_p by using winglets on wind turbines tested at Risø National
132 Laboratory, Denmark. A key aspect of their study was the utilisation of the geometry described by
133 Maughmer [10] which defined 8 key geometric parameters of winglets: height (relative to the blade
134 length), radius of curvature (relative to the winglet height), cant angle[†], toe angle, twist, aerofoil,

[†] As an unwritten convention, positive cant angles face the back of the turbine and negative ones to the front, The first ones have the same orientation as winglets on aeroplane wings.

135 chord distribution and sweep (Figure 2). Their initial study using the general-purpose incompressible
 136 Navier Stokes- solver EllipSys3D on winglets 1.5% (of blade length) high, a cant angle of 90° , and a
 137 sweep angle of 0° concluded that winglets could increase power coefficient by 1.3% while increasing
 138 the thrust coefficient 1.6% for the best configuration, that winglets affect approximately the outer
 139 14% of the blade, and that winglets facing downstream performed better. Further work by the same
 140 group using the same solver, provided analyses of 10 winglets facing downstream, with heights
 141 varying from 1-4%, curvature, radii 12.5-100%, twist angle up to 8° , and one with a sweep angle of
 142 30° . They found an increase in power of around 1.2% to 2.8%, with an increase in thrust coefficient
 143 (C_T) of 1.2% to 3.6% [16]. The study concluded that the power augmentation was a consequence of a
 144 reduction of tip effects, and not caused by the shift on downwind vorticity as it was believed until
 145 then. The idea that downwind winglets were superior was still supported. The studies were
 146 conducted using a Free Wake Lifting Line code and the CFD Navier-Stokes solver EllipSys3D [17].
 147



148
 149 Figure 2. Winglet geometry design variables.

150
 151 Over the last 15 years, more studies have been carried out, incorporating winglets of less than 10%
 152 of relative height with respect to the blade length, resulting in power coefficient increases ranging
 153 from 2% to 8%. Chattot [18] studied the effects of blade tip modifications on wind turbine
 154 performance using an optimization code, based on a numerical vortex model. The results favoured a
 155 backward sweep, and forward dihedral and winglet (facing upstream), with a height of 10%, giving a
 156 C_p increase of 3.5% at a TSR of 5.39. Lawton and Crawford [19] used a free wake vortex-based code
 157 and concluded that a winglet facing downwind of a 5% height would result in a power increase of 2%
 158 with a 2.8% increase in thrust. Elfarra *et al.* [20] used CFD to solve the Reynold savedged Navier
 159 Stokes (RANS) equations plus a genetic algorithm to optimize a winglet design of 1.5% height, 84°
 160 cant angle, 2° twist, and no apparent radius of curvature. The estimated power capture increase was
 161 9% and a 1.3% increase in the thrust coefficient. Subsequently, using the same computational
 162 method, it was reported that winglets add aerodynamic forces and bending moments due to their
 163 weight. Cant angles of 45° and 90° were analysed, with positive and negative sweeps. Within a TSR
 164 range of 1.57.5, a 3.24.6 increase in power coefficient was estimated and 0.81.5 increase in thrust
 165 coefficient [21].
 166

167 Gertz and Johnson [22] experimentally set a wind turbine baseline case for exchangeable tip designs
 168 for a 3.3 m diameter turbine. Then two winglet designs were evaluated, of 8% height, 90° cant angle,
 169 and -0.5° twist. The study showed a power increase of 5%-7% at a TSR of 6.7. Both winglets were
 170 found to have a bell-shaped power curve [23]. In a different experiment, the interaction between

171 two wind turbines fitted with winglets was studied. The wind turbine located downstream saw a
172 decrease in the power capture, however, the added power extraction of both was higher. Winglets
173 had a height of 6%, 90° cant angle, 1° twist, and -0.5° sweep angle. The increase in power coefficient
174 recorded was 4.2% at around a TSR of 6 and a 6.5% increase in thrust coefficient [24].

175

176 Mühle *et al.* [25] tested the effect of winglets on the tip vortex and the near wake, finding that for
177 wake regions larger than $x/D=4.0$, the wake's mean recovered faster due to the tip vortex
178 interaction stimulated by the winglets, in addition to a higher power extraction. Winglets were
179 designed with a height of 10.76%, a curvature radius of 3.09%, a cant angle of 90°, and a 17.86°
180 sweep angle. At a TSR of 6, the increase in power coefficient was 10.68% and 12.64% for the thrust
181 coefficient. The wind turbine manufacturer ENERCON is probably the only large manufacturer that
182 has exploited the potential of winglets. An example of this is the 2010 E-126 model, an upgraded
183 version of the 2007 E-126 model. The new model captured between 12% to 15% more energy by
184 refining the flow around the nacelle and by adding winglets [8].

185

186 Studies on winglets for tidal turbines are scarce, with most published work based on numerical
187 simulations. Most of the results produced a similar outcome that backwards-facing winglets should
188 perform better. Zhu *et al.* [26] took power and thrust measurements from an experimental study on
189 a horizontal axis marine turbine, carried out by Bahaj *et al.* [27] at the University of Southampton to
190 adjust their baseline for their RANS simulation. Their best simulated design produced a power
191 increase of 3.96% at a tip speed ratio of 7 and a pitch angle of 15° with a dual winglet of 2.5% height,
192 1.2% radius, 45° sweep, and each winglet facing the pressure and suction sides with cant angles of
193 90°. Ren *et al.* [28] proposed a triangular winglet bent downstream for their RANS equations
194 simulation. The results showed that winglets increased the power coefficient by 4.34% and the
195 thrust coefficient by 3.97% at an optimal TSR of 5. The design had a height of 6.3%, an 18:1 elliptical
196 tip of 10% the width of the winglet base aligned with the centreline of the blade, and a cant angle of
197 nearly 90°. In 2019, Ren *et al.* [29] also compared the effect of facing the winglets upstream and
198 downstream, finding that the best design achieved a 4.66% power increase when facing downstream
199 at a TSR of 4.2. The triangular winglets had a height of 5.3%, with a tip-to-base proportion of 84%,
200 and faced the suction side.

201

202 Young *et al.* [30] evaluated four different winglets, consisting of a linear extension of the tidal
203 turbine blade, varying the main parameter of cant angle. Two heights were considered, 10% and
204 20%, and relative curvature radii of 28% and 56% respectively. In their study, the power coefficient,
205 the hydrodynamic efficiency, and the structural efficiency were considered. After initial simulations
206 using a vortex lattice code called Tornado, three winglets were designed to face upstream, and one
207 downstream. In all cases it was hypothesized that blades with winglets perform better than the
208 regular blade. However, their results showed that only the winglets facing upstream did show better
209 performance. It was proposed that viscous effects (i.e., a separation at the corner of the blade-
210 winglet junction) play a role in the reduction in power coefficient for the winglet facing downstream.
211 A summary of the aforementioned studies is given in Table 1, an expanded list can be found in [31].

212

213 Most recently, Bayu and Shin [32] investigated the effect of winglets on a wind turbine using a RANS
214 model coupled with a $k-\omega$ SST turbulence model. Their configuration included winglets facing
215 upstream and downstream directions. Their best design had a 3%R height and a cant angle of -90°
216 (upstream configuration) with power coefficient increases of 1-2% and thrust coefficient increasing
217 by 1-3%. Dejene *et al.* [33] used a similar model to investigate the effect of winglets on the NREL
218 Phase VI wind turbine. Winglets were 0.7%R high, facing the suction side and with cant angles of 30°,
219 45° and 60°. Expected power generation increase ranges from 5% to 10% with thrust coefficients
220 increasing 7% - 8%. Wang *et al.* [34] performed a numerical and experimental study of a tidal turbine

221 with 10%R height and 60° bent winglet facing the direction of the current. The winglet configuration
222 improved the efficiency by 5.7% compared to the blade extension.

223

224 In summary, to date, there has been no consensus in the literature on the best direction of winglets
225 for horizontal axis tidal turbine blades – upstream or downstream – let alone more detailed
226 parameters such as height and curvature radius and their performance. This work is aimed at
227 providing more insights into the performance of a model tidal turbine with rotor blades fitted with
228 different winglets at different configurations tested experimentally.

229

230 **3. Experimental design, setup and calibration**

231

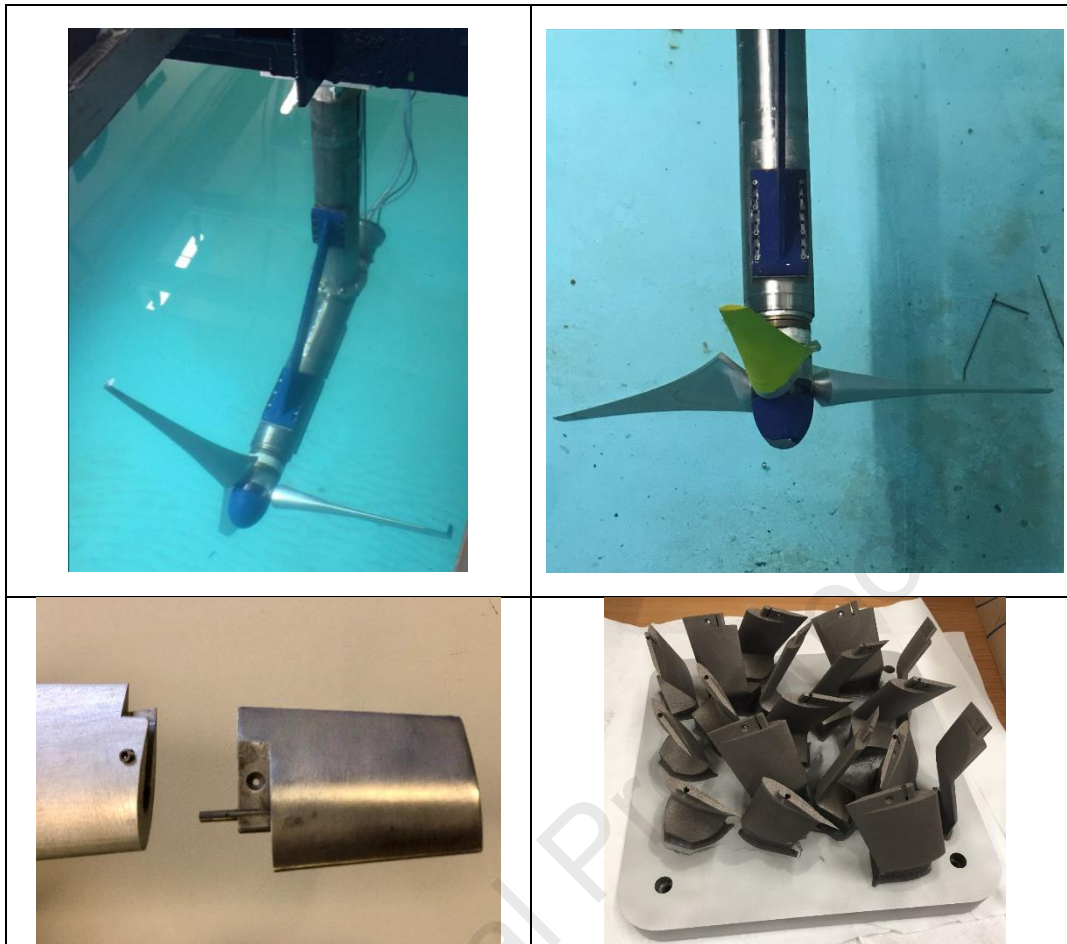
232 As part of this research, several winglets were designed, manufactured, and tested to provide an
233 understanding of the influence of varying winglet geometry on rotor thrust and power coefficients
234 as well as act as a benchmark for future work. The model turbine used in the experiments is a 3-
235 bladed ‘upwind’ horizontal axis device with a blade diameter of 1m (Figure 3). The turbine is fully
236 instrumented and equipped with a dynamometer that measures rotor torque and thrust at the hub.
237 It utilises full strain gauge bridges and runs ‘wet’ upstream of all seals and bearings [35]. Rotor speed
238 and blade radial position are quantified via a rotary encoder mounted on the main shaft within the
239 nacelle. A 2-stage planetary gearbox and a synchronous generator convert mechanical energy to
240 electrical and the rotor speed is controlled either by a wire-wound resistor bank or an electrical
241 variable load. All data travelling out from the turbine is sampled and amplified using a wireless
242 telemetry system to transmit data from the shaft to cables that join into a main umbilical cord that
243 also conveys the generated power out and low voltage DC power in to power the onboard systems.
244 Further details of the turbine design and general set-up can be found in [36,37]. The blade profile
245 geometry was provided by SIMEC Atlantis Energy Ltd. under an NDA, but a full tidal turbine blade
246 geometry can be found in [27]. The design was slightly modified to enable the tips to be
247 interchangeable, and the turbine has the capability to adjust the blade pitch from -5° to 5° in
248 increments of 1°.

249 Table 1 Studies on HATs with winglets and their design parameters

Research Paper				Parameters						Results		
Source	Type	Country	Method	Height [%R]	Radius [%H]	Cant [°]	T, t [‡] [°]	Sweep [°]	Aerofoil	TSR (λ)	P _{aug.} [%]	T _{aug.} [%]
Wang <i>et al.</i> , 2023	Tidal	China	Exp. + CFD	10		60			S809	3.5 – 8	5.7	
Dejene <i>et al.</i> , 2023	Wind	Ethiopia	RANS k-ω SST	0.7		-90			S809	7.5	5-10	7-8
Bayu and Shin, 2023	Wind	Japan	CFD-RANS	1.5-5		-90,90			S809		2.21	2.02
Young <i>et al.</i> , 2019	Tidal	UK	VLM + Exp.	10, 20	(10mm)	-90-90				4	10	
Ren <i>et al.</i> 2019	Tidal	China	CFD-RANS	5.3		-90, 90			NACA63-418	4.2	4.66	
Ren <i>et al.</i> 2017	Tidal	China	CFD-RANS	6.3		-75-90			NACA63-418	5	4.34	3.97
Zhu <i>et al.</i> , 2017	Tidal	China	CFD	2.5	48	-90, 90	-	45	NACA 63-812	3 - 10	3.96	
Ostovan and Uzol, 2016	Wind	Turkey	Exp.	6	(0)	90	1T	-0.5	PSU 94-097	~6	4.2	6.5
Elfarra, Sezer-Uzol and Akmandor, 2015	Wind	Turkey	CFD + GA	1.5	(0)	45, 90	0, 2T	+	S809	1.5-7.5	3.2-4.6	0.8-1.5
Lawton and Crawford, 2014	Wind	Canada	CFD	5		90	6.73T	0	NACA 64		~2	2.8
Elfarra, Sezer-Uzol and Akmandor, 2014	Wind	Turkey	CFD + GA	1.5	(0)	84	2T		S809		~9	~1.3
Gertz, Johnson and Swytink-Binnema, 2012	Wind	Canada	Exp.	8	(0)	90	-0.5T	0	PSU 94-097	6.7	5-7	
Chattot, 2009	Wind	USA	Num.	10	(0)	-90			S809	5.39	3.5	
Gaunaa and Johansen, 2007a	Wind	Denmark	Num.	2	25	90			Risø B1-15	8	2.47	2.61
Johansen and Sørensen, 2007	Wind	Denmark	CFD	2	20	90	4T	0			1.0-1.8	1.2-
Johansen and Sørensen, 2006	Wind	Denmark	CFD	1.5		90		0	NACA 64-518		1.3	1.6
Shimizu <i>et al.</i> , 2003	Wind	Japan	Exp.	9			Mie-type		NACA 4418	5.42	8.75	
van Bussel, 1990	Wind	Netherlands	Num.	20			Mie-type		NACA 4412	8	=	
Shimizu <i>et al.</i> , 1990	Wind	Japan	Exp.	~20			Mie-type		FX74-CL6-140	4	27	
Gyatt and Lissaman, 1985	Wind	USA	Exp.	5			Single, fin, and double		NACA 23012,21		-	

250

‡ T: twist, t: toe angle



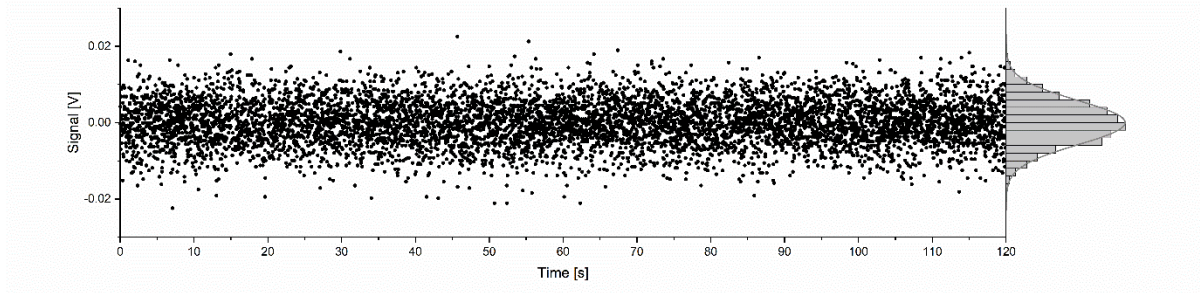
251 *Figure 3. Turbine installed in towing tank (Top left), main blade (Top right), blade and winglet interface (Bottom left),*
 252 *3D printed winglets (Bottom right).*

253 The blades were milled on a 5-axis CNC machine at the Engineering Design and Manufacturing
 254 Centre at the University of Southampton from T6082-T6 aluminium alloy, with an accuracy of ± 50
 255 microns. The winglets were 3D printed in aluminium at an accuracy of ± 0.1 mm, hand polished and
 256 finished.

257
 258 The thrust and torque signals were collected at a frequency of 67 Hz, filtered and amplified via a
 259 wireless telemetry system located inside the nacelle. A National Instruments® data acquisition (DAQ)
 260 box, model NI USB-6210, would receive the analogue signals, pass them to a LabVIEW® program for
 261 real-time viewing, and save the data for post-processing. The power was dissipated either by using
 262 an Aim-TTi LD300 Electronic Load or a 280-W rheostat.

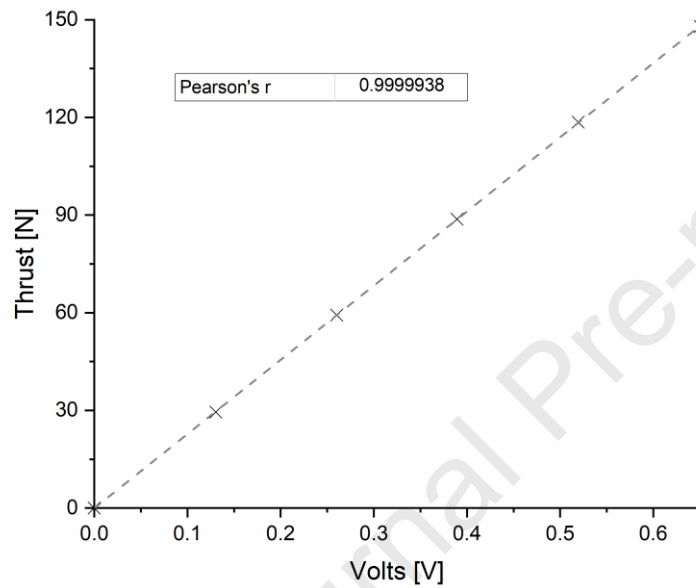
263
 264 The thrust dynamometer was calibrated from 0 to 150 N at intervals of 30 N with a precision of
 265 0.05 mN. The torque dynamometer calibration ranged from 0 to 11 N·m using intervals of 2.2 N·m
 266 measured to 0.02 mN·m, by hanging 0.5 kg weights at 0.442 ± 0.001 m from the centre of the shaft at
 267 $0 \pm 0.5^\circ$ at the plane of rotation. The zero reading for the thrust has scattered noise with a normal
 268 distribution as shown in the perpendicular histogram of Figure 4 with a standard deviation of
 269 ± 5.77 mV. The linear correlation has a value of 0.9999938 as shown in Figure 5. Measurement
 270 uncertainties are shown in Table 2. Precision has to do with the instrumentation and the regression
 271 uncertainty is derived from the calibration plot.

272



273
274 *Figure 4. Noise in the acquisition signal*

275
276

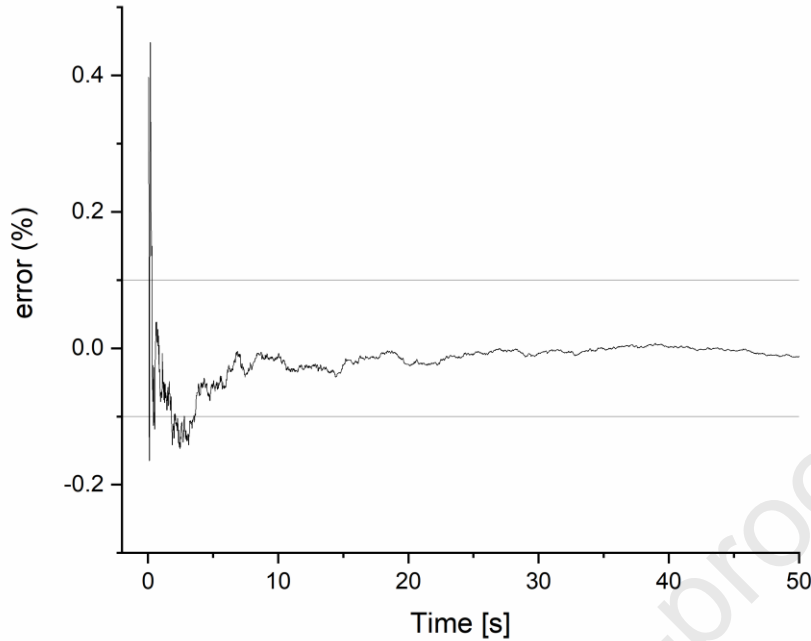


277
278 *Figure 5. Thrust calibration.*

279 *Table 2. Measurement uncertainties*

	Thrust (N)	Torque (N-m)	Ω (rpm)	Power (W)
Precision uncertainty	0.8538	0.0327	0.48	0.49
Regression uncertainty	0.4311	0.0257	-	-
Total uncertainty	0.9564	0.0416	0.48	0.49
Percentage of the mean	1.29%	0.77%	0.53%	1.30%

280
281 Averaging the signal over a period of 120s and plotting the error, the mean and the standard
282 deviation converge with an error of less than 0.1% in just under five seconds as can be seen in Figure
283 6. After performing the repeatability test, it was found that the revolutions per minute (rpm) can be
284 estimated around a predefined value with an accuracy of $\pm 0.48(02)$ rpm.
285



286
287 *Figure 6. Percentage error for a sample time of 2 minutes*

288 Experiments were conducted at the wave/towing tank at Solent University in Southampton, UK. The
289 tank has dimensions of 60 m long \times 3.7 m wide \times 1.8 m deep. The turbine was towed at 0.76 m/s,
290 allowing the turbine rotor to rotate within the range of 60–120 rpm. The towing speed was selected
291 to give a sufficient range of blade Tip Speed Ratio whilst being slow enough to maximise data
292 collection at a fixed acquisition frequency. The Froude number was approximately 0.137 (water
293 depth 3.5m, velocity 0.76 m/s), scaled to be representative of a real tidal channel and Reynolds
294 numbers of approximately 1.5×10^5 were observed at the tips of the blade (chord at scaled model of
295 0.0413 m) at an optimum rotational operation speed (TSR = 5). Towing faster resulted in minimal
296 change in performance curves (Re. independence), whilst decreasing time for data collection due to
297 length restriction. Depending on the winglet configuration, the rotational speeds chosen to
298 characterise the turbine were equivalent to values ranging from 4.5 to 7.5 TSR (λ).

299
300 The following standard equations are used to present non-dimensional rotor performance:
301

$$C_p = \frac{\text{Power}}{\frac{1}{2} \rho A u^3} \quad \text{Equation 1.}$$

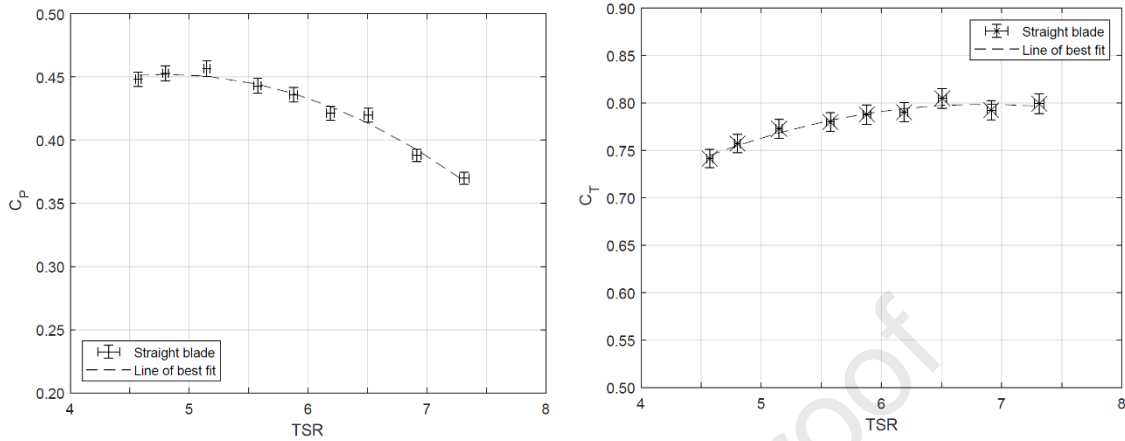
$$C_T = \frac{\text{Thrust}}{\frac{1}{2} \rho A u^2} \quad \text{Equation 2.}$$

$$TSR(\lambda) = \frac{\omega R}{u} \quad \text{Equation 3.}$$

302 Where ρ is the fluid density, A is the swept area of the rotor, u is the inflow velocity, ω is the
303 rotational speed in radians per second, and R is the rotor radius.

304 The characterisation of the turbine with the straight blade extensions (no winglets) for TSR from 4.5
305 to 7.5 is shown in Figure 7. The average value of C_p is 0.42, and C_T is 0.78, both values quoted for
306 further comparisons with winglets tests. Each TSR data point was obtained over a 1-min run to

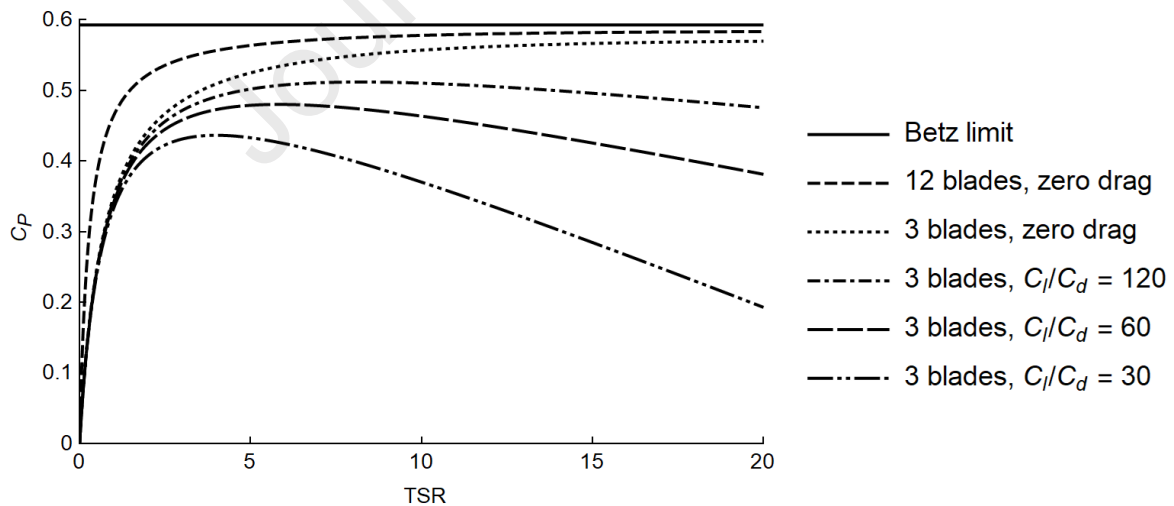
307 characterise the performance of the blades with winglets. Each run has a ramp-up period and a
 308 breaking period. In between these, a steady condition was achieved for approximately 30 seconds
 309 which generated over 2,000 data points at a sampling rate of 67 Hz. The error bars are calculated
 310 following the measurement uncertainties defined in Table 2.



311
 312 Figure 7. Tidal turbine C_p (Top) and C_T (Bottom) curves vs. TSR.

313 The maximum value of C_p is defined by the limit quantified by Betz [38] for a horizontal axis turbine
 314 which is equal to $16/27$ or 59.3% of the available power to the swept area of the rotor. In practice,
 315 C_p is used as a global or whole-device efficiency value and is applied at the rear of the turbine
 316 incorporating electrical and drivetrain losses but here it is applied at the rotor and can be measured
 317 using the dynamometer at the hub. Tip and hub losses are significant contributors to the difference
 318 between real rotor C_p and the Betz limit [35]. Figure 8, from formulae published by Wilson *et al.*
 319 (1976) [39], illustrates the effect of tip losses on rotor performance and thus efforts to reduce blade
 320 drag by minimising or completely eliminating tip losses that should be incorporated into the blade
 321 design.

322



323
 324 Figure 8. The variation of C_p with design TSR for various lift/drag ratios, zero drag and number of blades, where C_l and C_d
 325 are the coefficients of lift and drag respectively.

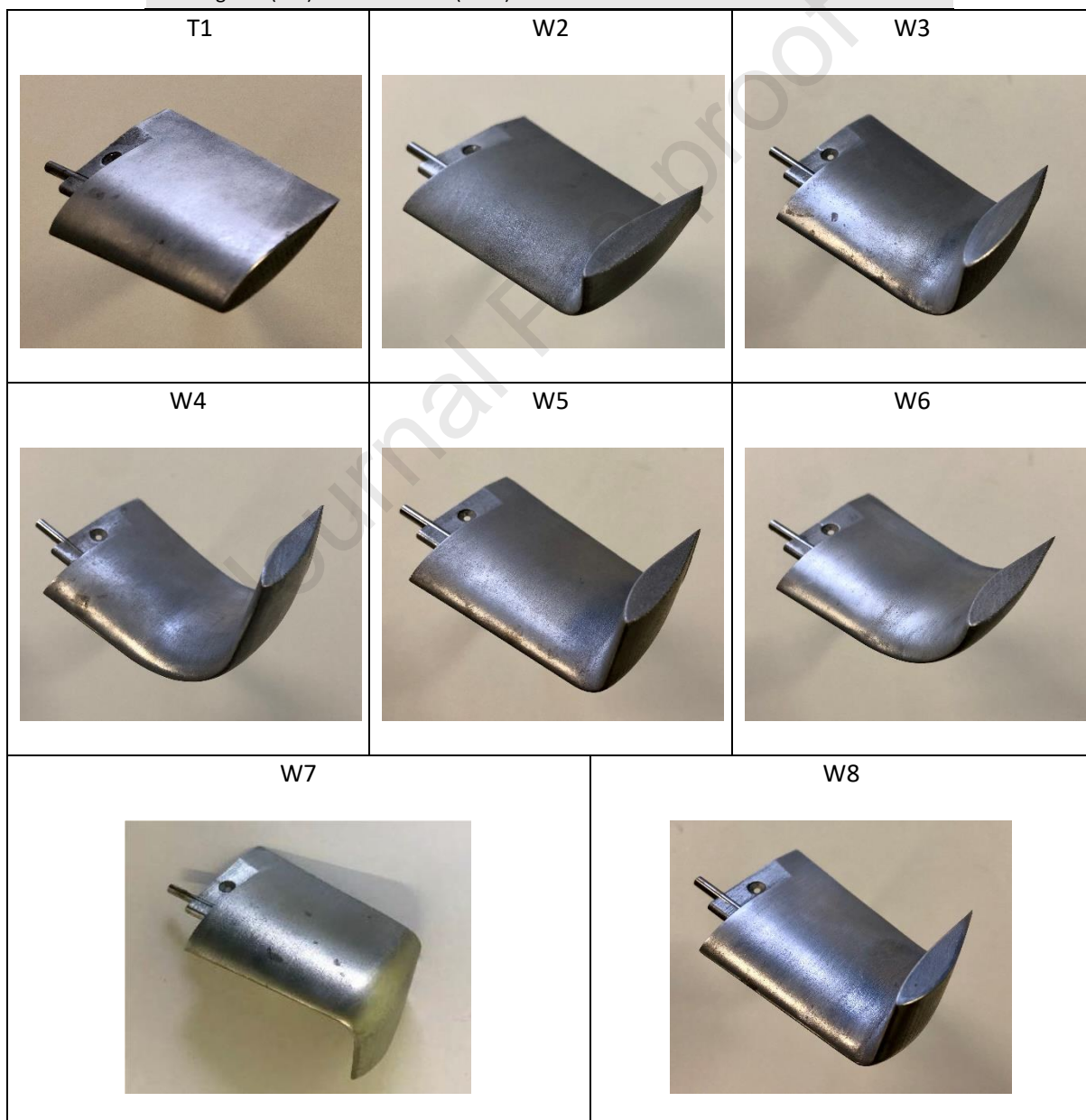
326 The design parameters of the winglets presented herein can be seen in Table 3. The three main
 327 parameters that could be compared between winglets were height, radius of curvature, and cant
 328 angle, plus aerofoil orientation (Figure 9). A positive cant angle means that the winglet is facing the
 329 suction side (backwards) and a negative angle that is facing the pressure side (forwards). In this

330 study the only winglet facing the front of the turbine is winglet 7. In all cases, the distance from the
 331 hub centre to the outer part of the blade is kept at constant 0.5 m.

332

333 *Table 3. Design parameters for selected winglets – see also Figure 9..*

Element	Height	Radius	Cant	Aerofoil
Blade tip (T1)	0 mm (0.0%)	0%	0°	Blade
Winglet 2 (W2)	12.5mm (2.5%)	50%	90°	Extension
Winglet 3 (W3)	25 mm (5.0%)	50%	90°	Extension
Winglet 4 (W4)	50 mm (10.0%)	50%	90°	Extension
Winglet 5 (W5)	25 mm (5.0%)	25%	90°	Extension
Winglet 6 (W6)	25 mm (5.0%)	100%	90°	Extension
Winglet 7 (W7)	25 mm (5.0%)	25%	-90°	Extension
Winglet 8 (W8)	25 mm (5.0%)	25%	90°	Inverted



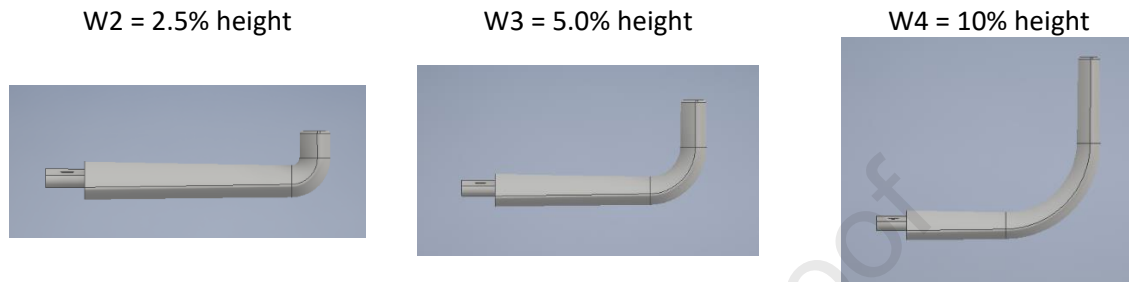
334 *Figure 9. Isometric view of winglets as described in Table 3. T1 is a blade tip. W2, W3, and W4 vary in height. W3, W5 and*
 335 *W6 have different curvature radii. W7 has an opposite cant angle but same geometry as W5. W8 has the same*
 336 *configuration as W5 as well but an inverted aerofoil which makes it a mirrored winglet to W7.*

337
338
339
340
341
342
343
344
345

4. Results and discussion

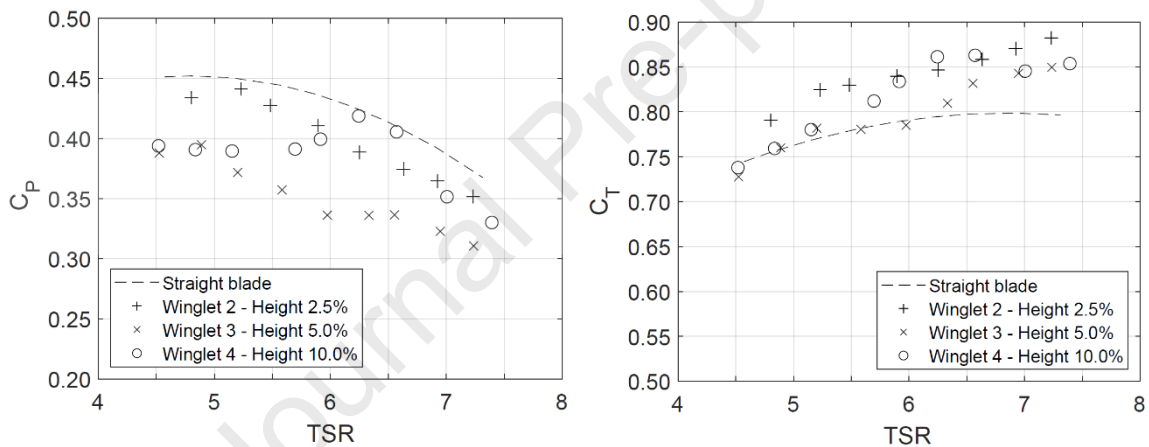
4.1 Winglet height

The first parameter to compare was winglet size. W2, W3 and W4 have a 2.5%, 5% and 10% height respectively, with a relative curvature radius of 50% (Figure 10).



346 Figure 10. Winglets 2, 3 and 4 (Table 3) with 2.5%, 5% and 10% height respectively with curvature radius of 50%.

347



348
349
350

Figure 11. Winglet performance in terms of C_p and C_t as a function of TSR, height and comparison with straight blade, all with relative radius curvature of 50%.

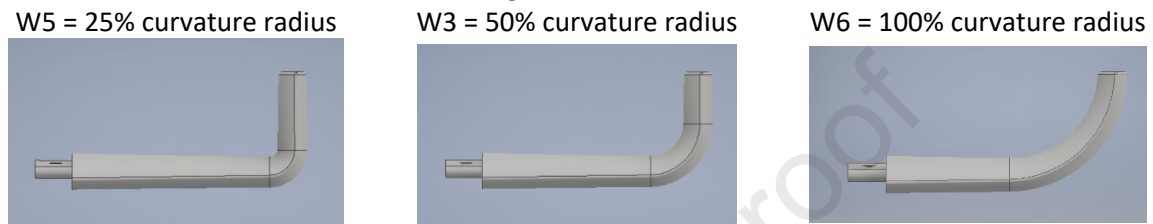
351 Figure 11 shows the winglet blade performance in terms of power (C_p) and thrust (C_t) coefficients for
352 different heights (Table 3) as a function of TSR. W2 has an average C_p value of 0.40, whilst W3 and
353 W4 had C_p at 0.35 and 0.38 respectively. These values are lower when compared with a straight
354 blade. Additionally, in all three cases, the thrust coefficient increased when compared with a straight
355 blade. This was contrary to the assumption that the reduction in induced drag during turbine
356 operation could outweigh the increase in profile drag due to the addition of winglets [20].
357 As can be seen in Figure 11, in terms of power coefficient (C_p) in all cases, the blade-winglet
358 configurations underperform compared to the straight blade. These results are in contrast to
359 previously published numerical studies on wind turbines [16,17,19], as well as the experimental
360 results from Ostovan and Uzol [24]. Computational simulations, specifically on tidal turbines, either
361 supported backwards-facing winglets or found no considerable difference regarding their
362 orientation, either facing forwards or backwards [26,29].

363
364
365
366
367

368
369
370
371
372
373
374
375
376
377
378
379

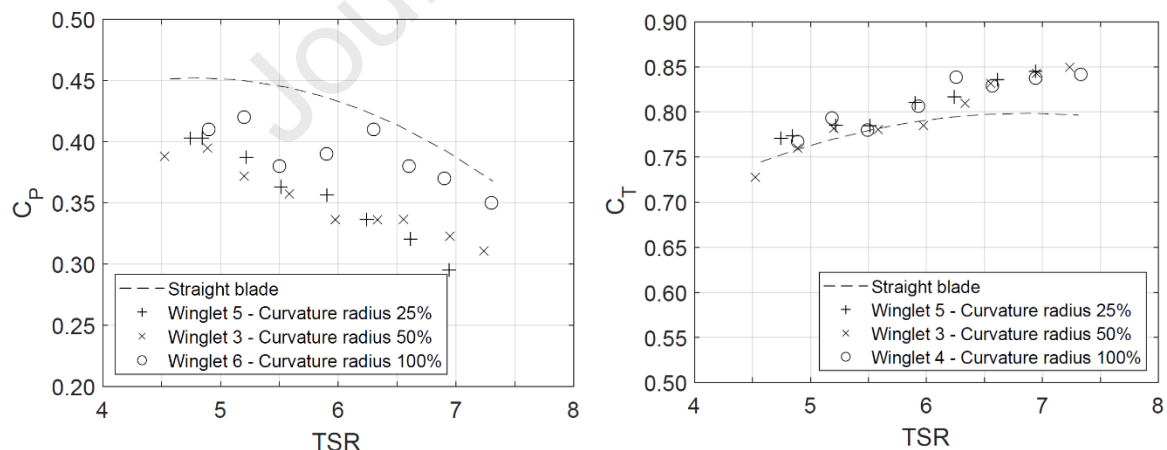
4.2 Winglet curvature radius

The second parameter to examine is the curvature radius. As shown in Figure 12 W5 has a 25% radius, W3 50%, and W6 100%, all with a height of 5%.



380 *Figure 12. Side view of winglets with same height, blade length and different curvature radii.*

381 Figure 13 depicts the winglet performance in terms of C_p and C_T as a function of TSR, curvature and comparison with straight blade, all with different radii and at height of 5%. It can be seen from the
382 figure that varying the radius of curvature from 25% to 50% C_p has almost identical values of 0.36 (W5) and 0.35 (W3) respectively. Whilst W6 at a 100% radius gave a relatively higher value of C_p of
383 0.39. In terms of C_p , all winglets still underperformed versus the straight blade. Previous studies
384 compared the influence of the radius on the power coefficient [16,17], favouring a curvature radius
385 of around 25%. At the design stage, the various winglets were designed with heights up to 10% and
386 curvature radii between 20% and 50%. In this experiment, winglets with different curvature radii did
387 not increase the power coefficient either, and there was no evident trend found as radius increased.
388
389
390

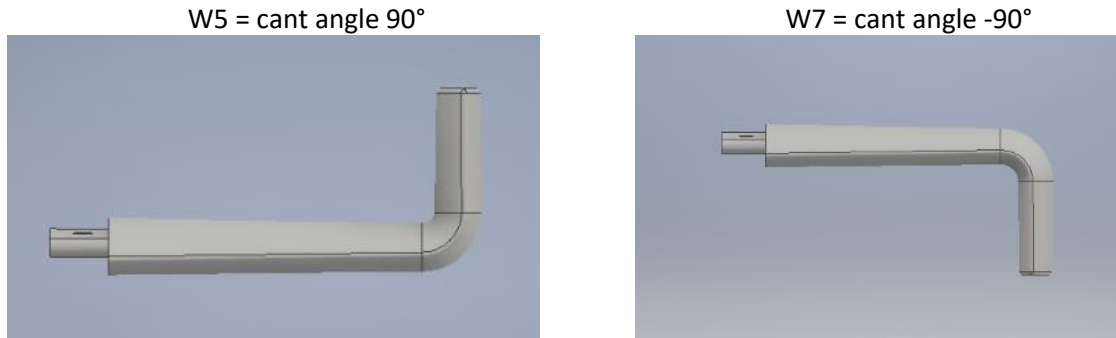


391 *Figure 13. Winglet performance in terms of C_p and C_T as a function of TSR, curvature and comparison with straight blade, all*
392 *with different radii and 5% height.*
393

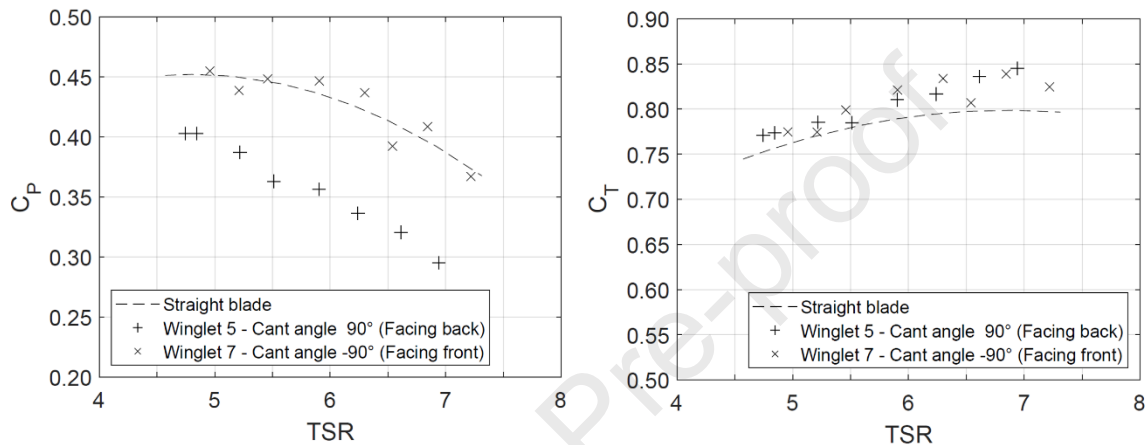
394 4.3 Winglet cant angle

395
396
397
398
399
400

The third parameter to compare is the cant angle between W5 and W7 (Figure 14). The design of W7
was initially carried out for completeness, as most previous studies had favoured backwards-facing
winglets. In fact, it turned out to be the first winglet with an evident difference in C_p , even
presenting a higher C_p than the straight blade at some regions, and eventually being key to
understanding other winglets' unexpected behaviour.



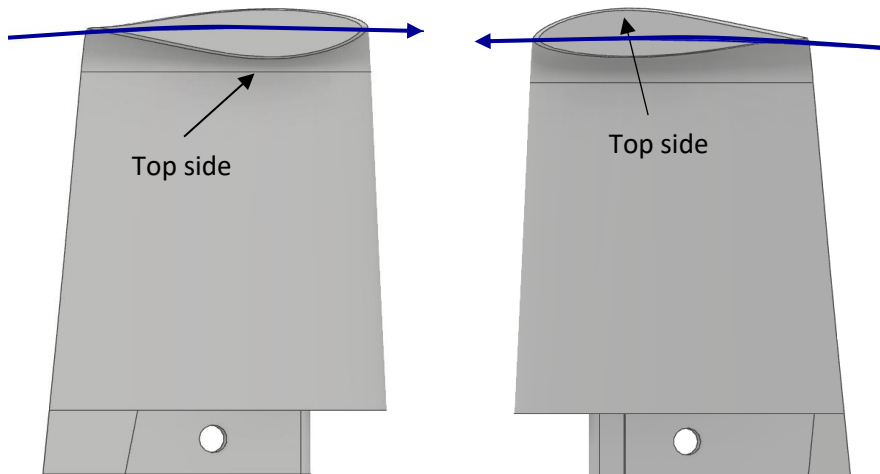
401 Figure 14. Winglets facing opposite sides of the turbine, where W5 is facing the suction side and W7 towards the pressure
402 side.



403 Figure 15. Power and thrust coefficient versus TSR for winglets facing opposite sides of the rotor showing the forward-
404 facing winglets improving C_p over backward-facing winglets and straight blade in some regions.
405

406 Figure 15 (Left) shows a significant difference between the power coefficient of W5, of 0.36 on
407 average (facing the suction side), and W7 with a value of 0.42 on average (facing the pressure
408 side), except from TSR 6 to 7 where there was an increase of 1-2%. At the same time, both thrust
409 coefficients have an average value of 0.80 and have higher values than those of the straight blade.

410 In this work, W7 presented the first winglet to show an increase in performance than the straight
411 blade (Figure 15). It has the same geometry as W5, but it is bent upstream towards the high pressure
412 side of the blade. The first assumption to explain this behaviour is that when winglets are bent to the
413 back of the rotor, the aerofoil ends up being upside down (Figure 16). It is assumed that an aerofoil
414 rotating with such orientation would have more resistance to motion than one in an upright
415 position.



416

417 *Figure 16. aerofoil orientation for opposite cant angles and blade radius of rotation, W5 (Left), W7 (Right).*

418 4.4 Winglet aerofoil orientation

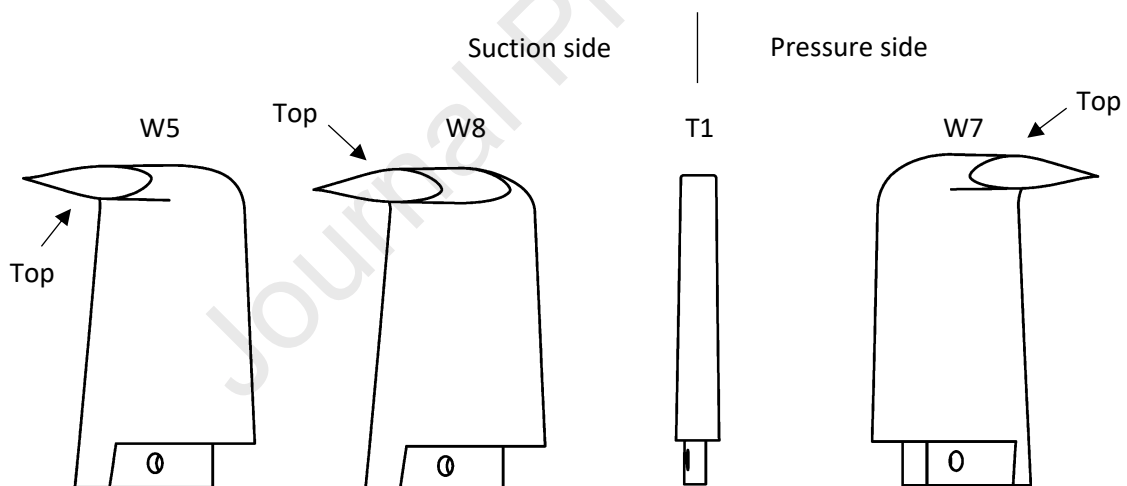
419

420 To compare the assumption made in the previous section, winglet W8 can be analysed. Its geometry
 421 is bent towards the back of the turbine as W5, with an inverted aerofoil. With such a configuration,
 422 the winglet ends up having a symmetrically-mirrored shape as W7 (Figure 17).

423

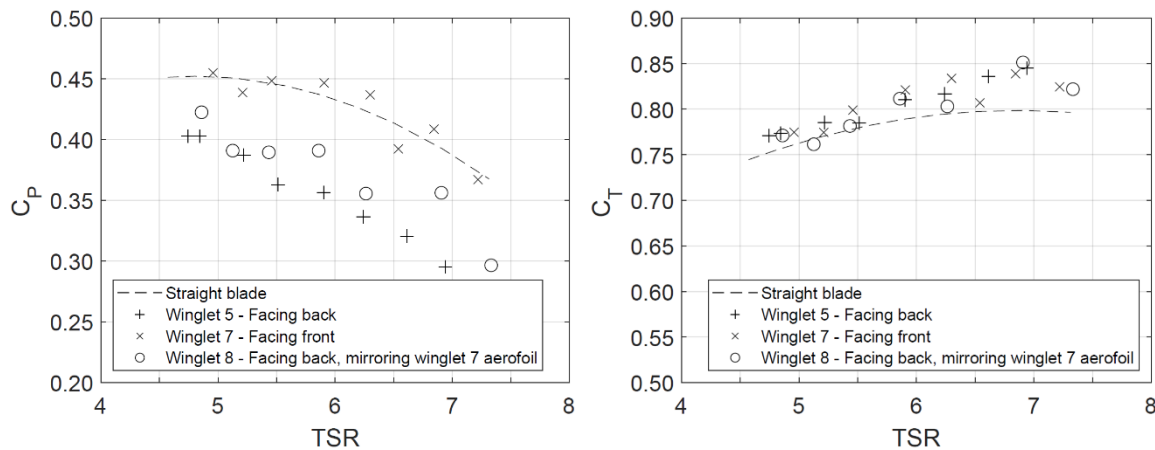
424

425



426

427 *Figure 17. Aerofoil orientation for W5, W7 and W8.*



428
429
430
431
432

Figure 18. C_p and C_T curves versus TSR for opposite cant angles. W7 is bent towards the front, while W5 is bent towards the back, by doing so, the aerofoils end up inversed to each other. Winglet 8 is similar to W5, with an inverted aerofoil, so it has the same orientation as W7 that is facing the front. This allows a direct comparison between cant angles for winglets facing opposite directions, as the aerofoil on both W7 and W8 have the same spatial orientation.

433
434
435
436
437
438
439
440

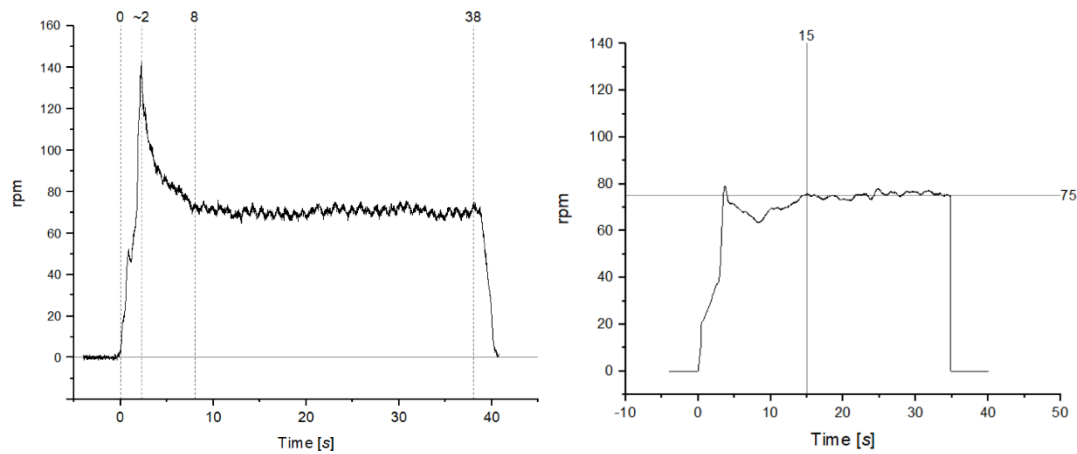
Figure 18, shows the results of changing the aerofoil orientation to allow a more significant comparison for the cant angle. The average C_p value of W5 is 0.36, W8 0.37 and W7 0.42. All winglets had an average C_T of 0.80. So, the difference in average C_p between W7 and W5 with opposite cant angles cannot be solely attributed to aerofoil orientation. Previous studies suggested that winglets facing the pressure side performed better than the ones oriented towards the suction side, Chattot [18] with an optimization code based on a numerical vortex model, and Young [30] using a vortex lattice method.

441
442

4.5 Surface flow visualisation

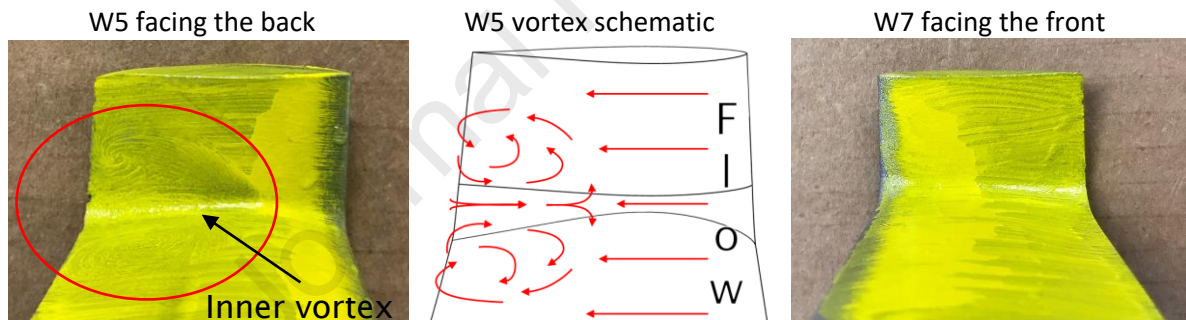
443
444
445
446
447
448
449
450
451
452
453
454
455
456
457

Following the quantification of rotor power and thrust performance, an oil-based paint flow visualisation technique was used to study the flow on the surface of the winglets near peak C_p at a TSR of 5.0 to visualise the flow on the surface of the two symmetrical winglets W7 and W8 facing opposite directions, looking for an explanation on why W7 facing the front had a better performance than W8, which is geometrically mirrored but facing towards the back of the turbine. An example of the technique can be seen in [40]. In these experiments, oil-based paint was combined with flaxseed oil, and by trial and error a dilution ratio of 2:1 was found to have the right viscosity for a TSR of 5. Under normal testing the rotor was artificially started to overcome starting torque which resulted in a peak RPM greater than steady operation. For the runs with flow visualisation the starting procedure was modified to ensure the maximum and steady RPM only occurred during the steady operation period. Figure 19 (Left) shows a normal test run where the carriage acceleration produces a spike in the turbine speed. Figure 19 (Right) is the plot of the modified run to avoid such abrupt increase. It can also be noticed that the time to reach a steady speed almost doubles, steady speed time lasts less than in a normal run (as no data is processed), and instead of a gradual stop of the carriage, the turbine is left to stop on its own



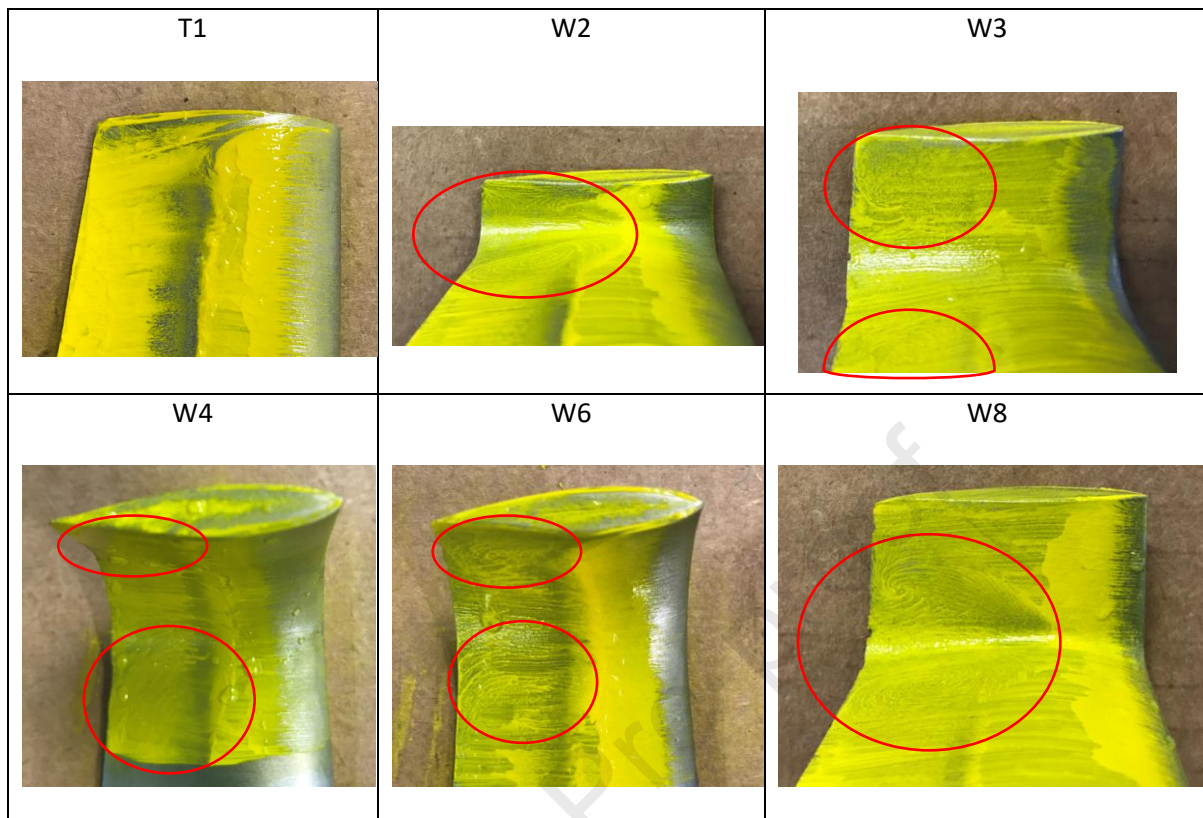
458
459 *Figure 19. Normal experimental run (Left). Modified run for flow visualisation tests (Right).*

460 As can be seen in Figure 20 (Left), it was identified that the phenomenon behind the
 461 underperformance of all winglets, except W7, was a vortical flow structure being formed at the
 462 blade-winglet interface. The schematic of the vortex is shown in Figure 20 (Centre), produced by a
 463 large flow detachment from the surface. The same behaviour was found in all winglets facing the
 464 suction side (Figure 21). That is what was impeding the winglets from enhancing the power capture
 465 and in fact reducing the power coefficient compared to a straight blade. However, in the case of W7,
 466 there was no such vortex found as can be observed in Figure 20 (Right). All photographs were
 467 captured immediately after each run by bringing the turbine out of the water and removing the
 468 winglets.
 469



470 *Figure 20. Oil-based paint flow visualisation of a vortex behind winglets facing the suction side (Left), vortex*
 471 *schematic (Centre), and no vortex towards the pressure side (Right).*

472



474 *Figure 21. Oil flow visualisation for T1 and the rest of the winglets facing the back (suction side).*

475

476 Judging from Figure 21, the difference in the performance of backward-facing winglets is attributed
 477 to vortices that vary in shape and size, not only per configuration but most probably for the same
 478 winglet at different speeds. Taking W2, W3 and W4, it can be seen that as the winglet increases in
 479 size, so does the vortex, with the difference that W3 and W4 seem to have either a split vortex or
 480 two of them. The more pronounced radius of curvature seems to be responsible for such an effect. A
 481 better understanding of the vortices could be achieved by using flow visualisation in 3D that includes
 482 the flow away from the winglet surface.

483

484

5. Conclusions

485 In recent years, numerical simulations using CFD have sought to predict the effect that blade tip
 486 winglets might have on the power and thrust coefficients of horizontal axis wind turbines. Such
 487 predictions suggested that the addition of winglets could increase the power coefficient in a range
 488 from 2% to 8%. The three main design parameters varied were height, curvature radius and cant
 489 angle. Winglet heights of up to 10% had been favoured, with relative curvature radii of around 25%
 490 and up to 50%, and a cant angle of 90° (facing the suction side). Until now only disparate
 491 experimental work has been conducted and very few studies concerning tidal turbines.

492 This work presents a series of experiments using a 1m-diameter 3-bladed horizontal axis tidal
 493 turbine equipped to measure rotor thrust, torque, rotational speed, and blade position. A range of
 494 winglet designs were manufactured and tested to quantify the effect of varying winglet height,
 495 radius, and cant angle. It was found that all winglet geometries tested that faced the suction side of
 496 the blade decrease the power coefficient compared to a reference straight blade. With the use of an
 497 oil-based paint flow visualisation, it was possible to identify vortical flow structures and areas of flow

498 separation where winglets interface with the tip of the straight portion of the blade; Features that
499 are unlikely to be simulated using inviscid numerical models.

500 An increase in power coefficient of 1-2% was measured for a symmetrical winglet facing the
501 pressure side of the blade together with an increase in the thrust coefficient of up to 3-4%.

502 The addition of winglets could provide meaningful increases in power capture for a marginal
503 increase in capital cost with no additional increase in rotor diameter. Adding winglets might be more
504 favourable than increasing rotor diameter to increase power as the latter brings blades into closer
505 proximity with sheared flow close to the seabed and wave motion near the surface and the resultant
506 increase in dynamic loading.

507 This work quantifies the performance of a range of winglet designs and gives some insight into why
508 certain designs located on the suction side of the blade underperform compared to previous
509 numerical simulations. Numerical models that can simulate and more accurately quantify the effects
510 of rotational flow and separation are recommended for any continuing work in this area. This work
511 also provided some experimental evidence of enhancements of performance and to this end, further
512 work is being planned to expand the range of winglets that can be used and to explore additional
513 geometric properties including winglets orientated upstream on the pressure side of the blade.

514 **Acknowledgements**

515

516 PhD funded by the Department of Energy in Mexico (SENER), managed by the Mexican National
517 Council of Science and Technology (CONACyT) on energy sustainability CONACyT-SENER. The authors
518 kindly thank Atlantis Resources Ltd., now SIMEC Atlantis Energy Ltd., for providing the blade profile
519 geometry. Prof. Stephen Turnock for his encouragement on the exploration of the flow around the
520 winglets, and Dr. Roeland de Kat for his guidance on paint-based surface flow visualisation.

521 **Data Availability**

522 Datasets related to this article can be found at <http://dx.doi.org/10.5258/SOTON/D2129>, hosted at
523 ePrints Soton (Olvera Trejo, Rodolfo (2022) Winglets. University of Southampton).

524 **References**

525

526 [1] UK Government, National Renewable Energy Action Plan for the United Kingdom, (2010) 1–
527 160.

528 [https://www.gov.uk/government/uploads/system/uploads/attachment_data/file/47871/25-](https://www.gov.uk/government/uploads/system/uploads/attachment_data/file/47871/25-nat-ren-energy-action-plan.pdf)
529 [nat-ren-energy-action-plan.pdf](https://www.gov.uk/government/uploads/system/uploads/attachment_data/file/47871/25-nat-ren-energy-action-plan.pdf) (accessed August 11, 2022).

530 [2] European Commission, Plan REPowerEU, (2022) 21.

531 https://ec.europa.eu/commission/presscorner/detail/en/IP_22_3131 (accessed August 11,
532 2022).

533 [3] UK Government, British Energy Security Strategy, (2022).

534 [https://assets.publishing.service.gov.uk/government/uploads/system/uploads/attachment_d](https://assets.publishing.service.gov.uk/government/uploads/system/uploads/attachment_data/file/1069969/british-energy-security-strategy-web-accessible.pdf)
535 [ata/file/1069969/british-energy-security-strategy-web-accessible.pdf](https://assets.publishing.service.gov.uk/government/uploads/system/uploads/attachment_data/file/1069969/british-energy-security-strategy-web-accessible.pdf) (accessed August 11,
536 2022).

537 [4] A.S. Bahaj, Generating electricity from the oceans, Renewable and Sustainable Energy
538 Reviews 15 (2011) 3399–3416. <https://doi.org/10.1016/j.rser.2011.04.032>.

- 539 [5] A.S. Bahaj, Marine current energy conversion: the dawn of a new era in electricity
540 production, *Philosophical Transactions of the Royal Society* 371 (2013).
541 <https://doi.org/10.1098/rsta.2012.0500>.
- 542 [6] BEIS, Contracts for Difference Allocation Round 4 results, (2022) 1–9.
543 [https://assets.publishing.service.gov.uk/government/uploads/system/uploads/attachment_d](https://assets.publishing.service.gov.uk/government/uploads/system/uploads/attachment_data/file/1088875/contracts-for-difference-allocation-round-4-results.pdf)
544 [ata/file/1088875/contracts-for-difference-allocation-round-4-results.pdf](https://assets.publishing.service.gov.uk/government/uploads/system/uploads/attachment_data/file/1088875/contracts-for-difference-allocation-round-4-results.pdf) (accessed August
545 11, 2022).
- 546 [7] Ocean Energy Systems, Annual Report 2019, (2019) 152.
547 <https://tethys.pnnl.gov/publications/ocean-energy-systems-annual-report-2019> (accessed
548 August 11, 2022).
- 549 [8] E. de Vries, Close up - Enercon, super turbines and beyond, *Windpower Monthly* (2010).
550 [https://www.windpowermonthly.com/article/1047013/close-enercon-super-turbines-](https://www.windpowermonthly.com/article/1047013/close-enercon-super-turbines-beyond)
551 [beyond](https://www.windpowermonthly.com/article/1047013/close-enercon-super-turbines-beyond) (accessed August 11, 2022).
- 552 [9] R.T. Whitcomb, A design approach and selected wind tunnel results at high subsonic speeds
553 for wing-tip mounted winglets, *Nasa Tn D-8260* (1976) 1–33.
554 <https://ntrs.nasa.gov/archive/nasa/casi.ntrs.nasa.gov/19760019075.pdf> (accessed August 11,
555 2022).
- 556 [10] M.D. Maughmer, Design of Winglets for High-Performance Sailplanes, *J Aircr* 40 (2003) 1099–
557 1106. <https://doi.org/10.2514/2.7220>.
- 558 [11] G.W. Gyatt, P.B.S. Lissaman, Development and testing of tip devices for horizontal axis wind
559 turbines, (1985). <https://ntrs.nasa.gov/search.jsp?R=19860009304> (accessed August 11,
560 2022).
- 561 [12] Y. Shimizu, G.J. Van Bussel, S. Matsumura, A. Bruining, K. Kikuyama, Y. Hasegawa, Studies on
562 Horizontal Axis Wind Turbines With Tip Attachments, *Proc. of European Community Wind*
563 *Energy Conference* (1990) 279–283.
- 564 [13] G.J.W. van Bussel, A momentum theory for winglets on horizontal axis windturbine rotors
565 and some comparison with experiments, *4th IEA Symp. on the Aerodynamics of Wind*
566 *Turbines* (1990).
- 567 [14] Y. Shimizu, E. Ismaili, Y. Kamada, T. Maeda, Power augmentation of a HAWT by Mie-type tip
568 vanes, considering wind tunnel flow visualisation, blade-aspect ratios and Reynolds number,
569 *Wind Engineering* 27 (2003) 183–194. <https://doi.org/10.1260/030952403769016663>.
- 570 [15] J. Johansen, N. Sørensen, Aerodynamic investigation of Winglets on Wind Turbine Blades
571 using CFD, *Riso-R-1543(EN)* 1543 (2006).
- 572 [16] J. Johansen, N. Sørensen, Numerical analysis of winglets on wind turbine blades using CFD,
573 *European Wind Energy Conference and Exhibition* (2007).
- 574 [17] M. Gaunaa, J. Johansen, Determination of the Maximum Aerodynamic Efficiency of Wind
575 Turbine Rotors with Winglets, *J Phys Conf Ser* 75 (2007) 012006.
576 <https://doi.org/10.1088/1742-6596/75/1/012006>.
- 577 [18] J.-J. Chattot, Effects of blade tip modifications on wind turbine performance using vortex
578 model, *Comput Fluids* 38 (2009) 1405–1410.
579 <https://doi.org/10.1016/j.compfluid.2008.01.022>.

- 580 [19] S. Lawton, C. Crawford, Investigation and Optimization of Blade Tip Winglets Using an Implicit
581 Free Wake Vortex Method, *J Phys Conf Ser* 524 (2014) 012033. [https://doi.org/10.1088/1742-](https://doi.org/10.1088/1742-6596/524/1/012033)
582 [6596/524/1/012033](https://doi.org/10.1088/1742-6596/524/1/012033).
- 583 [20] M.A. Elfarra, N. Sezer-Uzol, İ.S. Akmandor, NREL VI rotor blade: numerical investigation and
584 winglet design and optimization using CFD, *Wind Energy* 17 (2014) 605–626.
585 <https://doi.org/10.1002/we.1593>.
- 586 [21] M.A. Elfarra, N. Sezer-Uzol, İ.S. Akmandor, Investigations on Blade Tip Tilting for Hawt Rotor
587 Blades Using CFD, *Int J Green Energy* 12 (2015) 125–138.
588 <https://doi.org/10.1080/15435075.2014.889007>.
- 589 [22] D. Gertz, D.A. Johnson, An evaluation testbed for wind turbine blade tip designs-baseline
590 case, *Int J Energy Res* 35 (2011) 1360–1370. <https://doi.org/10.1002/er.1897>.
- 591 [23] D. Gertz, D. Johnson, N. Swytink-Binnema, An Evaluation Testbed for Wind Turbine Blade Tip
592 Designs - Winglet Results, *Wind Engineering* 36 (2012) 389–410.
593 <https://doi.org/10.1260/0309-524X.36.4.389>.
- 594 [24] Y. Ostovan, O. Uzol, Experimental Study on the Effects of Winglets on the Performance of
595 Two Interacting Horizontal Axis Model Wind Turbines, *J Phys Conf Ser* 753 (2016) 022015.
596 <https://doi.org/10.1088/1742-6596/753/2/022015>.
- 597 [25] F. Mühle, J. Bartl, T. Hansen, M.S. Adaramola, L. Sætran, An experimental study on the effects
598 of winglets on the tip vortex interaction in the near wake of a model wind turbine, *Wind*
599 *Energy* 23 (2020) 1286–1300. <https://doi.org/10.1002/we.2486>.
- 600 [26] B. Zhu, X. Sun, Y. Wang, D. Huang, Performance characteristics of a horizontal axis turbine
601 with fusion winglet, *Energy* 120 (2017) 431–440.
602 <https://doi.org/10.1016/j.energy.2016.11.094>.
- 603 [27] A.S. Bahaj, A.F. Molland, J.R. Chaplin, W.M.J. Batten, Power and thrust measurements of
604 marine current turbines under various hydrodynamic flow conditions in a cavitation tunnel
605 and a towing tank, *Renew Energy* 32 (2007) 407–426.
606 <https://doi.org/10.1016/j.renene.2006.01.012>.
- 607 [28] Y. Ren, B. Liu, T. Zhang, Q. Fang, Design and hydrodynamic analysis of horizontal axis tidal
608 stream turbines with winglets, *Ocean Engineering* 144 (2017) 374–383.
609 <https://doi.org/10.1016/j.oceaneng.2017.09.038>.
- 610 [29] Y. Ren, B. Liu, T. Zhang, Influences of winglets on the hydrodynamic performance of
611 horizontal axis current turbines, *Applied Ocean Research* 92 (2019) 101931.
612 <https://doi.org/10.1016/j.apor.2019.101931>.
- 613 [30] A.M. Young, A.S.M. Smyth, V. Bajpai, R.F. Augarde, J.R. Farman, C.L. Sequeira, Improving tidal
614 turbine efficiency using winglets, in: *13th European Wave and Tidal Energy Conference 2019*,
615 2019: pp. 1–11.
- 616 [31] R. Olvera Trejo, An experimental study on the effects of winglets on the performance of
617 horizontal axis tidal turbines, University of Southampton, 2022.
- 618 [32] B.K. Wardhana, B.R. Shin, NUMERICAL INVESTIGATION OF THE EFFECT OF WINGLET
619 CONFIGURATIONS ON THE BLADE PERFORMANCE FOR HORIZONTAL AXIS WIND TURBINE, in:

- 620 Proceeding of 8th Thermal and Fluids Engineering Conference (TFEC), Begellhouse,
621 Connecticut, 2023: pp. 783–786. <https://doi.org/10.1615/TFEC2023.eet.045960>.
- 622 [33] G. Dejene, V.R. Ancha, A. Bekele, NREL Phase VI wind turbine blade tip with S809 airfoil
623 profile winglet design and performance analysis using computational fluid dynamics, Cogent
624 Eng 11 (2024). <https://doi.org/10.1080/23311916.2023.2293562>.
- 625 [34] Y. Wang, B. Guo, F. Jing, Y. Mei, Hydrodynamic Performance and Flow Field Characteristics of
626 Tidal Current Energy Turbine with and without Winglets, J Mar Sci Eng 11 (2023) 2344.
627 <https://doi.org/10.3390/jmse11122344>.
- 628 [35] T. Blackmore, L.E. Myers, A.S. Bahaj, Effects of turbulence on tidal turbines: Implications to
629 performance, blade loads, and condition monitoring, International Journal of Marine Energy
630 14 (2016) 1–26. <https://doi.org/10.1016/j.ijome.2016.04.017>.
- 631 [36] A.S. Bahaj, L.E. Myers, Shaping array design of marine current energy converters through
632 scaled experimental analysis, Energy 59 (2013) 83–94.
633 <https://doi.org/10.1016/j.energy.2013.07.023>.
- 634 [37] P.W. Galloway, L.E. Myers, A.B.S. Bahaj, Quantifying wave and yaw effects on a scale tidal
635 stream turbine, Renew Energy 63 (2014) 297–307.
636 <https://doi.org/10.1016/j.renene.2013.09.030>.
- 637 [38] A. Betz, Das maximum der theoretisch moglichen Auswendung des Windes durch
638 Windmotoren, Zeitschrift Fur Gesamte Turbinewesen 26 (1920).
- 639 [39] J.F. Manwell, J.G. McGowan, A.L. Rogers, Wind Energy Explained: Theory, Design and
640 Application, Wiley, 2010.
- 641 [40] C.M. Harwood, Y.L. Young, S.L. Ceccio, Ventilated cavities on a surface-piercing hydrofoil at
642 moderate Froude numbers: cavity formation, elimination and stability, J Fluid Mech 800
643 (2016) 5–56.

644

Declaration of interests

The authors declare that they have no known competing financial interests or personal relationships that could have appeared to influence the work reported in this paper.

The authors declare the following financial interests/personal relationships which may be considered as potential competing interests:

Journal Pre-proof